International Journal of Mechanical Sciences 134 (2017) 500–510

Contents lists available at ScienceDirect

International Journal of Mechanical Sciences

journal homepage: www.elsevier.com/locate/ijmecsci

Gaussian and non-Gaussian stochastic response of slender continua with time-varying length deployed in tall structures

Stefan Kaczmarczyk[a,*], Radosław Iwankiewicz[b,c]

[a] The University of Northampton, St. George's Avenue, Northampton NN2 6JD, United Kingdom
[b] Hamburg University of Technology, Eissendorfer Strasse 42, D-21073 Hamburg, Germany
[c] The University of Zielona Gora, Poland

ARTICLE INFO

Keywords:
Cable vibration
Structure sway
Time-variant system
Transient resonance
Narrow-band Gaussian stochastic process
Random pulse train

ABSTRACT

This paper presents a study to predict the probabilistic characteristics of lateral dynamic motions of a long heavy cable moving at speed within a tall host structure. The cable is subjected to a base-motion (kinematic) excitation due to a low frequency sway of the structure. The development of the deterministic equations of motion and of the stochastic models describing the lateral dynamic behaviour of the cable is presented. Due to the time-varying length of the cable, the system exhibits nonstationary dynamic characteristics and its response is governed by nonstationary ordinary differential equations. Two stochastic models of motion of the structure are considered. In the first model, the excitation is represented as a narrow-band Gaussian process mean-square equivalent to a harmonic process. The second model involves a non-Gaussian process in the form of a random train of pulses, idealizing the action of strong wind gusts. The differential equations to determine the mean values and the second-order joint statistical moments of the response are formulated and solved numerically. A parametric study is conducted to demonstrate the influence of speed of the cable on the deterministic and stochastic characteristics of the response.

1. Introduction

Environmental phenomena such as strong wind conditions and earthquakes cause tall civil structures such as towers and high-rise buildings to vibrate (sway) at low frequencies and large amplitudes [1,2]. When the structure is sufficiently flexible, the dynamic response to forces generated by these phenomena is significant. As a result, the corresponding kinematic excitation often excites long slender continua such as cables and ropes that are part of equipment hosted within the structure. For example, large resonance motions of suspension ropes and compensating cables in high-speed elevators in high-rise buildings take place [3]. In order to predict the dynamic behaviour of moving continua in such systems, various models have been used. The excitation mechanism can be represented by deterministic functions and consequently the response of the system is treated as a deterministic phenomenon [4–8]. However, the nature of loading caused by environmental phenomena such as wind is usually nondeterministic [9,10]. The excitation should then be described by a stochastic process so that the methods of stochastic dynamics can be employed to predict the dynamic behaviour of the system.

In this work, the model and stochastic methodology proposed by Kaczmarczyk et al. [11] is extended and used to carry out a comprehensive computer simulation study to predict the dynamic response of a long cable moving at speed within a tall slender host structure. First, a derivation of the deterministic model which describes the dynamic behaviour of the system is summarized and the dynamic characteristics of the system are explained. Two, stochastic models of motion of the structure are considered. In the first model, the excitation is represented as a narrow-band Gaussian process mean-square equivalent to a harmonic process. Alternatively, the dynamic loading due to wind gusts may be adequately idealized by a train of randomly occurring pulses [12–14] with the corresponding the dynamic response of a structure being also a train of pulses. Hence, in the second model, the excitation is treated as a non-Gaussian process in the form of a random train of pulses. For both models, the non-stationary differential equations governing the statistical moments of the state vector are presented. The

* Corresponding author.
E-mail addresses: stefan.kaczmarczyk@northampton.ac.uk (S. Kaczmarczyk), iwankiewicz@tu-harburg.de (R. Iwankiewicz).

https://doi.org/10.1016/j.ijmecsci.2017.10.030
Received 7 February 2017; Received in revised form 14 October 2017; Accepted 23 October 2017
Available online 25 October 2017

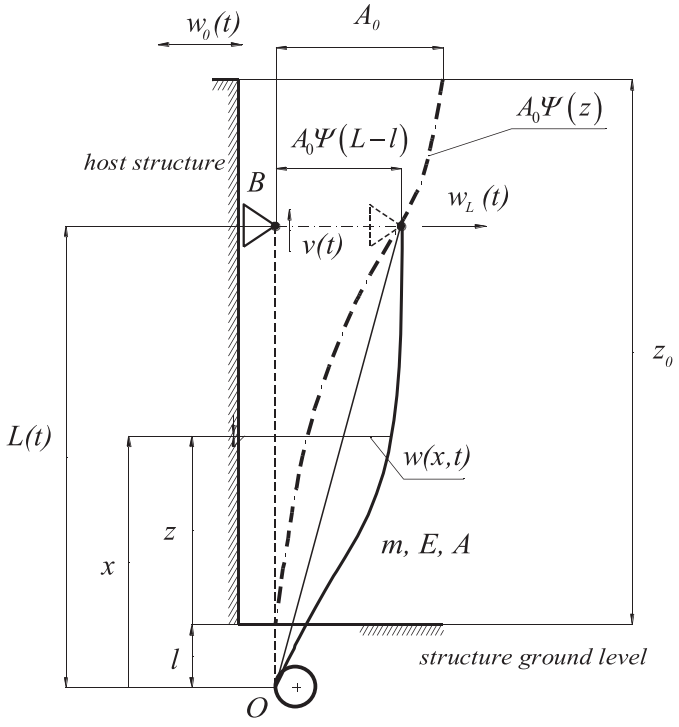

Fig. 1. Vertical cable moving within a tall structure.

equations are then solved numerically and a numerical study based on a range of model parameters of the system is conducted.

2. Equations of motion

The model depicted in Fig. 1 is used to study the dynamic behaviour of a vertical cable of time-varying length $L(t)$. The cable which has mass per unit length m is wrapped around a drum at the bottom end and attached at B to a support moving at speed v within a tall cantilevered host structure. The host structure sways which results in motion $w_0(t)$ of amplitude A_0 at the level defined by the coordinate z_0 measured from the structure base level. The deformations of the structure are described as $A_0\Psi(z)$ where $\Psi(z)$ represents the deformation shape function with z denoting a coordinate measured from the base level. The base motion $w_0(t)$ excites the cable and its dynamic response is represented by the lateral displacements denoted as $w(x,t)$, where x is measured from the origin O placed at distance l below the base level.

The equations of motion of the system presented in what follows are based on the model discussed in [11], with a more accurate representation of the deformations of the structure used. The mean quasi-static tension of the cable is expressed as

$$T_m(x,t) = T_0 + mx[g + a(t)] \tag{1}$$

where the spatial coordinate x is defined in a time-variant domain $0 < x < L(t)$, T_0 represents a constant tension term, $a(t) = \dot{v}(t)$ is the acceleration of the upper support (an overdot denotes the time derivative) and g is the acceleration of gravity.

The equation governing the linear undamped dynamic response of the cable in terms of the lateral displacements $w(x,t)$ is given as

$$m\frac{\mathrm{d}^2 w}{\mathrm{d}t^2} - \left[T_0 + m(g+a)x\right]w_{xx} - m(g+a)w_x = 0 \tag{2}$$

where $()_x$ denotes partial derivatives with respect to x and

$$\frac{\mathrm{d}^2 w}{\mathrm{d}t^2} = w_{tt} + 2vw_{xt} + v^2 w_{xx} + aw_x \tag{3}$$

where $()_t$ denotes partial derivatives with respect to time.

The displacements at the boundaries $x = 0$, $L(t)$ are defined as

$$w(0,t) = 0, \mathrm{w[L(t),t]=w_L}(t) \tag{4}$$

where $w_L(t)$ represents lateral displacements of the structure corresponding to the upper end of the cable (see Fig. 1). The continuous system described by Eqs. (2)–(4) is discretized using the following approximation of the solution:

$$w(x,t) = \bar{w}(x,t) + W_0(x,t), \quad 0 \le x \le L(t) \tag{5}$$

where

$$\bar{w}(x,t) = \sum_{n=1}^{N} \Phi_n[x; L(t)]q_n(t), \quad 0 \le x \le L(t) \tag{6}$$

is an approximate solution that satisfies homogenous boundary conditions with $\Phi_n[x; L(t)]$ representing the nth eigenfunction of a taut string of instantaneous length $L = L(t)$ with a constant tension. The eigenfunctions are given as

$$\Phi_n[x; L(t)] = \sin\frac{n\pi}{L(t)}x, \quad n = 1, 2, \ldots, N \tag{7}$$

and $q_n(t)$ represents the nth modal coordinate. $W_0(x,t)$ is a particular solution that satisfies the non-homogenous boundary conditions (4). Noting that the lateral displacements at $x = L(t)$ can be expressed as $w_L(t) = \Psi_L[L(t)]w_0(t)$, where $\Psi_L = \Psi[L(t) - l]$, the particular solution is given as

$$W_0(x,t) = \mathrm{Y}[x; L(t)]w_0(t), \quad 0 \le x \le L(t) \tag{8}$$

where $\mathrm{Y}[x; L(t)] = \Psi_L[L(t)]\frac{x}{L(t)}$. In this model, the deformation shape function $\Psi(z)$ is assumed to be related to the fundamental mode of the structure and is approximated by a cubic polynomial as follows:

$$\Psi(z) = 3\left(\frac{z}{z_0}\right)^2 - 2\left(\frac{z}{z_0}\right)^3 \tag{9}$$

so that the deformation shape at $z = L(t) - l$ is expressed as

$$\Psi_L[L(t)] = 3\left(\frac{L(t)-l}{z_0}\right)^2 - 2\left(\frac{L(t)-l}{z_0}\right)^3 \tag{10}$$

respectively. It can be assumed that the length L is a *slowly varying* parameter, i.e. that its variation is observed on a *slow time* scale defined as $\tau = \varepsilon t$, where $\varepsilon \ll 1$ is a small quantity [15]. Thus, $L = L(\tau)$ and the rate of change of L with respect to time t is proportional to ε

$$\frac{dL}{dt} \equiv \dot{L} = \frac{dL(\tau)}{d\tau}\frac{d\tau}{dt} = \varepsilon\frac{dL(\tau)}{d\tau}; \quad \ddot{L} = \varepsilon^2\frac{d^2L(\tau)}{d\tau^2} \tag{11}$$

Consequently, noting that $v \equiv \dot{L}$, $a = \ddot{L}$ the velocity and acceleration can also be considered as being slowly varying. Using Eq. (11) the expressions for partial derivatives with respect to time t of the expression (5) are given as

$$w_t = \sum_{n=1}^{N}\left\{\varepsilon\frac{dL(\tau)}{d\tau}\frac{\partial\Phi_n[x; L(\tau)]}{\partial L}q_n(t) + \Phi_n[x; L(\tau)]\dot{q}_n(t)\right\} + \varepsilon\frac{dL(\tau)}{d\tau}\frac{\partial \mathrm{Y}[x; L(\tau)]}{\partial L}w_0(t) + \mathrm{Y}[x; L(\tau)]\dot{w}_0(t); \tag{12a}$$

$$w_{tt} = \sum_{n=1}^{N}\left\{\begin{aligned}&\varepsilon^2\left[\left(\frac{dL(\tau)}{d\tau}\right)^2\frac{\partial^2\Phi_n[x;L(\tau)]}{\partial L^2} + \frac{d^2L(\tau)}{d\tau^2}\frac{\partial\Phi_n[x;L(\tau)]}{\partial L}\right]q_n(t)\\ &+2\varepsilon\frac{dL(\tau)}{d\tau}\frac{\partial\Phi_n[x;L(\tau)]}{\partial L}\dot{q}_n + \Phi_n[x; L(\tau)]\ddot{q}_n\end{aligned}\right\}$$
$$+\varepsilon^2\left\{\left(\frac{dL(\tau)}{d\tau}\right)^2\frac{\partial^2\mathrm{Y}[x; L(\tau)]}{\partial L^2} + \frac{d^2L(\tau)}{d\tau^2}\frac{\partial \mathrm{Y}[x; L(\tau)]}{\partial L}\right\}w_0(t)$$
$$+2\varepsilon\frac{dL(\tau)}{d\tau}\frac{\partial \mathrm{Y}[x; L(\tau)]}{\partial L}\dot{w}_0(t) + \mathrm{Y}[x; L(\tau)]\ddot{w}_0(t); \tag{12b}$$

$$\bar{w}_{xt} = \sum_{n=1}^{N}\left\{\varepsilon\frac{dL(\tau)}{d\tau}\frac{\partial\Phi'_n[x; L(\tau)]}{\partial L}q_n(t) + \Phi'_n[x; L(\tau)]\dot{q}_n(t)\right\} + \varepsilon\frac{dL(\tau)}{d\tau}\frac{\partial \mathrm{Y}'[x; L(\tau)]}{\partial L}w_0(t) + \mathrm{Y}'[x; L(\tau)]\dot{w}_0(t), \tag{12c}$$

where the primes denote partial derivatives with respect to x. By using (6)–(12) in (5), substituting the result in (2), multiplying by $\Phi_r[x; L(\tau)]$,

integrating the result and orthogonalising with respect to the natural modes, when terms $O(\varepsilon)$ and $O(\varepsilon^2)$ are neglected, the following set of ordinary differential equations results

$$\ddot{q}_r(t) + \sum_{n=1}^{N} C_{rn}(\tau)\dot{q}_n(t) + \sum_{n=1}^{N} K_{rn}(\tau)q_n(t) = Q_r(t;\tau), \quad r = 1, 2, \ldots, N \tag{13}$$

where the slowly varying coefficients $K_{rn}(\tau)$, $C_{rn}(\tau)$ and the modal excitation function $Q_r(t;\tau)$ are given as

$$C_{rn}(\tau) = \begin{cases} 2\varsigma_r\bar{\omega}_r(\tau), & n = r \\ \frac{4nrv(\tau)}{(n^2-r^2)L(\tau)}\left((-1)^{r+n}-1\right), & n \neq r \end{cases},$$

$$K_{rn}(\tau) = \begin{cases} \bar{\omega}_r^2(\tau) - \frac{r^2\pi^2}{L(\tau)}\left[\frac{v^2(\tau)}{L(\tau)} - \frac{g+a(\tau)}{2}\right], & n = r \\ \frac{2}{(n^2-r^2)L(\tau)}\left[\frac{2rn^3(g+a(\tau))}{n^2-r^2} - grn\right]\left[(-1)^{r+n}-1\right], & n \neq r \end{cases}$$

$$Q_r(t;\tau) = \frac{2\Psi_L}{r\pi L(\tau)}\left\{(-1)^r L(\tau)\ddot{w}_0(t) - \left[gw_0(t) - 2v\dot{w}_0(t)\right]\left[(-1)^r - 1\right]\right\} \tag{14}$$

where r, $n = 1, 2, \ldots, N$, $\bar{\omega}_r(\tau) = \frac{r\pi}{L(\tau)}\sqrt{\frac{T_0}{m}}$ and ς_r represents the modal damping ratios of the cable. Eq. (13) with slowly varying coefficients describe the nonstationary dynamic behaviour of the system. An adverse situation arises when the structure is excited near its fundamental natural frequency. This in turn leads to a passage through resonance in the cable system [4,15] when one of its slowly time-varying natural frequencies approaches that of the inertial load resulting from the resonance sway.

3. Stochastic models

3.1. Narrow-band Gaussian stochastic model

It can be assumed that $w_0(t)$ is an oscillatory motion with frequencies within a narrow range of the centre frequency Ω_0. Thus, $w_0(t)$ is considered as a narrow band, an almost harmonic process, mean-square equivalent to the (harmonic) process with the amplitude A_0 and the frequency Ω_0. It should be noted that the process $w_0(t)$ which represents the structural displacement response, must be twice differentiable, i.e. its first- and second-order derivatives $\dot{w}_0(t)$ and $\ddot{w}_0(t)$, respectively, must exist [9]. This scenario is adequately idealized by assuming that the motion $w_0(t)$ is the response of the second order auxiliary filter to the process $X(t)$, which in turn is the response of the first-order filter to the Gaussian white noise excitation $\xi(t)$ [11]. The governing equations are

$$\begin{aligned} \ddot{w}_0(t) + 2\zeta_f\Omega_0\dot{w}_0(t) + \Omega_0^2 w_0(t) &= X(t) \\ \dot{X}(t) + \alpha X(t) &= \alpha\sqrt{2\pi S_0}\xi(t) \end{aligned} \tag{15}$$

where ζ_f denotes the damping ratio of the filter which defines its band width, α is the filter variable, S_0 is the constant level of the power spectrum of white noise $\xi(t)$. To be more exact, the response $X(t)$ to the Gaussian white noise excitation $\xi(t)$ is a process which is not differentiable in the usual sense; hence, the notation $\dot{X}(t)$ is not mathematically meaningful. The second equation in (15) has a clear mathematical sense when it is written in the differential form. Accordingly, the governing equations for both filters are written down in a state space form as

$$\mathrm{d}\begin{bmatrix} X \\ w_0 \\ \dot{w}_0 \end{bmatrix} = \begin{bmatrix} -\alpha & 0 & 0 \\ 0 & 0 & 1 \\ 1 & -\Omega_0^2 & -2\zeta_f\Omega_0 \end{bmatrix}\begin{bmatrix} X \\ w_0 \\ \dot{w}_0 \end{bmatrix}\mathrm{d}t + \begin{bmatrix} \alpha\sqrt{2\pi S_0} \\ 0 \\ 0 \end{bmatrix}\mathrm{d}W(t) \tag{16}$$

where $\mathrm{d}W(t)$ is the increment of the Wiener process $W(t)$ and the Gaussian white noise excitation $\xi(t)$ is the generalized (not in usual sense) derivative of the Wiener process. In this representation the stochastic process, $w_0(t)$ is mean-square equivalent to the harmonic process if its standard deviation and variance are given as

$$\sigma_{w_0} = \frac{\sqrt{2}}{2}\mathrm{A}_0, \quad \mathrm{var}(w_0) = \sigma_{w_0}^2 = \frac{A_0^2}{2} \tag{17}$$

respectively. It can be shown that this equivalence is achieved if the filter variable α is given as [9]

$$\alpha = \Omega_0\left(-\zeta_f + \sqrt{\zeta_f^2 + \frac{\zeta_f\Omega_0^3A_0^2}{\pi S_0 - \zeta_f\Omega_0^3A_0^2}}\right) \tag{18}$$

It is important to note that the choice of parameters in Eq. (18) should guarantee that the filter variable α is real. It is evident from the last equation in Eq. (14) that the excitation function $Q_r(t;\tau)$ can be expressed in terms of the motion $w_0(t)$ and its time derivatives as

$$Q_r(t;\tau) = \beta_r^{(1)}(\tau)w_0(t) + \beta_r^{(2)}(\tau)\dot{w}_0(t) + \beta_r^{(3)}(\tau)\ddot{w}_0(t) \tag{19}$$

where

$$\begin{aligned} \beta_r^{(1)}(\tau) &= -2g\frac{\Psi_L[L(\tau)]}{r\pi L(\tau)}\left[(-1)^r - 1\right] \\ \beta_r^{(2)}(\tau) &= 4v\frac{\Psi_L[L(\tau)]}{r\pi L(\tau)}\left[(-1)^r - 1\right] \\ \beta_r^{(3)}(\tau) &= 2\frac{\Psi_L[L(\tau)]}{r\pi}(-1)^r \end{aligned} \tag{20}$$

Using the first equation (15) the second derivative of $w_0(t)$ can be expressed as

$$\ddot{w}_0(t) = X(t) - \Omega_0^2 w_0(t) - 2\zeta_f\Omega_0\dot{w}_0(t) \tag{21}$$

so that Eq. (19) can be rewritten as

$$Q_r(t;\tau) = \gamma_r^{(1)}(\tau)w_0(t) + \gamma_r^{(2)}(\tau)\dot{w}_0(t) + \beta_r^{(3)}(\tau)X(t) \tag{22}$$

where

$$\begin{aligned} \gamma_r^{(1)} &= \beta_r^{(1)} - \Omega_0^2\beta_r^{(3)} \\ \gamma_r^{(2)} &= \beta_r^{(2)} - 2\zeta_f\Omega_0\beta_r^{(3)} \end{aligned} \tag{23}$$

The state vector defined as

$$\mathbf{Y}(t) = \left[\mathbf{q}(t) \;\; \dot{\mathbf{q}}(t) \;\; X(t) \;\; w_0(t) \;\; \dot{w}_0(t)\right]^T \tag{24}$$

where $\mathbf{q} = [q_1, q_2, \ldots, q_N]^T$, is then governed by the following set of stochastic equations:

$$\mathrm{d}\mathbf{Y}(t) = \mathbf{A}\mathbf{Y}(t)\mathrm{d}t + \mathbf{b}\mathrm{d}W(t) \tag{25}$$

where

$$\mathbf{A} = \begin{bmatrix} \mathbf{0} & \mathbf{I} & \mathbf{0} \\ -\mathbf{K} & -\mathbf{C} & \mathbf{B} \\ \mathbf{0} & \mathbf{0} & \mathbf{A}_f \end{bmatrix}, \quad \mathbf{b} = \begin{bmatrix} \mathbf{0} \\ \mathbf{0} \\ \mathbf{b}_f \end{bmatrix} \tag{26}$$

with $\mathbf{I}$ denoting the identity matrix and $\mathbf{K}$ and $\mathbf{C}$ representing the matrices of coefficients $K_{rn}(\tau)$ and $C_{rn}(\tau)$ appearing in Eq. (13), respectively. Furthermore, $\mathbf{B}$ is a matrix with rows comprising coefficients $\beta_r^{(3)}, \gamma_r^{(1)}, \gamma_r^{(2)}$ and the matrix $\mathbf{A}_f$ and vector $\mathbf{b}_f$ in (26) are defined as follows:

$$\mathbf{B} = \begin{bmatrix} \beta_1^{(3)} & \gamma_1^{(1)} & \gamma_1^{(2)} \\ \beta_2^{(3)} & \gamma_2^{(1)} & \gamma_2^{(2)} \\ \cdots & \cdots & \cdots \\ \beta_N^{(3)} & \gamma_N^{(1)} & \gamma_N^{(2)} \end{bmatrix} \tag{27}$$

$$\mathbf{A}_f = \begin{bmatrix} -\alpha & 0 & 0 \\ 0 & 0 & 1 \\ 1 & -\Omega_0^2 & -2\zeta_f\Omega_0^2 \end{bmatrix}, \quad \mathbf{b}_f = \begin{bmatrix} \alpha\sqrt{2\pi S_0} \\ 0 \\ 0 \end{bmatrix} \tag{28}$$

As the increments of the Wiener process are zero-mean, i.e. $E[\mathrm{d}W(t)] = 0$, and the system is governed by the linear stochastic Eq. (25), it follows that the mean values of the state variables are zero-mean as well, $E[\mathbf{Y}(t)] = 0$. The differential equations governing the second-order statistical moments of the state vector, i.e. the covariance matrix $\mathbf{R}_{\mathbf{YY}} = E[\mathbf{Y}\mathbf{Y}^T]$, with its elements expressed as $\mu_{ij} = E[Y_i(t)Y_j(t)]$, are then obtained from Eq. (25) and are written in the following form:

$$\frac{\mathrm{d}}{\mathrm{d}t}\mathbf{R}_{\mathbf{YY}} = \mathbf{A}\mathbf{R}_{\mathbf{YY}} + \mathbf{R}_{\mathbf{YY}}\mathbf{A}^T + \mathbf{b}\mathbf{b}^T \tag{29}$$

The variance of the lateral displacement can then be determined as

$$\sigma_w^2(x,t) = E\left[\bar{w}^2(x,t)\right] = E\left\{\sum_{i=1}^{N}\sum_{j=1}^{N}\Phi_i[x;L(\tau)]\Phi_j[x;L(\tau)]q_i(t)q_j(t)\right\} \quad (30)$$

Furthermore, higher-order joint statistical moments of the state vector $\mathbf{Y}(t)$ can be determined with the aid of Itô's differential rule [16].

3.2. Motion of a structure as a random pulse train

Alternatively, it can be assumed that the motion $w_0(t)$ is due to randomly occurring strong wind gusts. An adequate idealization of this motion is the random train of pulses

$$w_0(t) = \sum_{i=1}^{N(t)} s(t-t_i) \quad (31)$$

where $s(t-t_i)$ is the motion (response) of the structure due to a single pulse (gust) of a strong wind and $N(t)$ is a homogenous Poisson counting process, giving the random number of occurrence times $t_i \in [0,\ t)$, i.e. excluding the possible occurrence at t.

The structure can be idealized by considering its fundamental mode so that it is represented as a single-degree-of-freedom system. The motion $w_0(t)$ is then governed by the following equation:

$$\ddot{w}_0(t) + 2\zeta_0\Omega_0\dot{w}_0(t) + \Omega_0^2 w_0(t) = X(t) \quad (32)$$

where Ω_0 is the fundamental natural frequency and ζ_0 is the modal damping ratio of the structure. In this model, the function $X(t)$ represents a stochastic excitation process in the form of train of pulses representing the wind gusts. This process is conveniently modelled as the response of an auxiliary 2nd order filter to a Poisson train of impulses, governed by the equation

$$\ddot{X}(t) + 2\zeta_f\Omega_f\dot{X}(t) + \Omega_f^2 X(t) = \sum_{i=1}^{N(t)} P_i\delta(t-t_i) \quad (33)$$

where P_i are the magnitudes of impulses assumed to be mutually independent random variables, identically distributed and also statistically independent of the random occurrence time t_i, or of the counting process $N(t)$. Here, Ω_f and ζ_f are the natural frequency and the damping ratio of the auxiliary filter, respectively. Hence, the process $X(t)$ is a train of impulse response functions $h(t-t_i)$ of the filter given as

$$X(t) = \sum_{i=1}^{N(t)} P_i h(t-t_i) \quad (34)$$

where $h(t-t_i)$ represents the response of a filter to a single Dirac delta impulse $\delta(t-t_i)$, defined by the following equation:

$$h(t-t_i) = \frac{1}{\Omega_f\sqrt{1-\zeta_f^2}}\exp\left[-\zeta_f\Omega_f(t-t_i)\right]\sin\left[\Omega_f\sqrt{1-\zeta_f^2}(t-t_i)\right], \quad t > t_i \quad (35)$$

Thus, the motion $s(t-t_i)$ is the response of the structure to the pulse $P_i h(t-t_i)$.

If the damping ratio ζ_f of the filter is assumed to be close to the unity, the function $h(t)$ becomes practically a single pulse, with an insignificant tail. Duration of such a single pulse is $T_f = \pi/(\Omega_f\sqrt{1-\zeta_f^2})$ and depends on the frequency of the filter and may be related to the natural period of the structure. Fig. 2(a) illustrates the impulse response function plotted vs. time with $t_i = 0$, $\Omega_f = \Omega_0 = 0.7854$ rad/s (0.125 Hz) and $\zeta_f = 0.5$. The impulse response function maximum value $h_{max} = 0.6956$ corresponds to the time $t_{max} = 1.5396$ s and $T_f = 4.6188$ s. Fig. 2(b) shows the impulse response function when $\Omega_f = 2.4\Omega_0 = 1.8850$ rad/s (0.3 Hz) and $\zeta_f = 0.95$. The maximum value of the impulse is then $h_{max} = 0.2019$ which corresponds to the time instant $t_{max} = 0.5395$ s and the duration time is $T_f = 5.3376$ s.

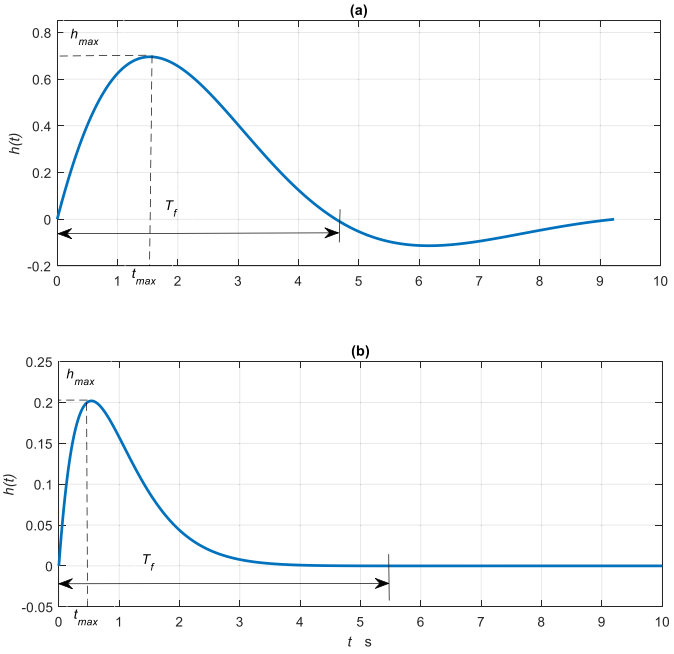

Fig. 2. Impulse response function plotted vs. time, (a) $\Omega_f = \Omega_0 = 0.7854$ rad/s (0.125 Hz) and $\zeta_f = 0.5$; (b) $\Omega_f = 2.4\ \Omega_0 = 1.8850$ rad/s (0.3 Hz) and $\zeta_f = 0.95$.

The displacements $w_0(t)$ and the process $X(t)$ are described by Eqs. (32) and (33), respectively, are then governed by the following stochastic equations:

$$\begin{aligned} dX(t) &= \dot{X}(t)dt \\ d\dot{X}(t) &= -2\zeta_f\Omega_f\dot{X}(t)dt - \Omega_f^2 X(t)dt + P(t)dN(t) \\ dw_0(t) &= \dot{w}_0(t)dt, \\ d\dot{w}_0(t) &= -2\zeta_0\Omega_0\dot{w}_0(t)dt - \Omega_0^2 w_0(t)dt + X(t)dt \end{aligned} \quad (36)$$

In the matrix form, the stochastic equations are written as

$$d\begin{bmatrix} X \\ \dot{X} \\ w_0 \\ \dot{w}_0 \end{bmatrix} = \begin{bmatrix} 0 & 1 & 0 & 0 \\ -\Omega_f^2 & -2\zeta_f\Omega_f & 0 & 0 \\ 0 & 0 & 0 & 1 \\ 1 & 0 & -\Omega_0^2 & -2\zeta_0\Omega_0 \end{bmatrix}\begin{bmatrix} X \\ \dot{X} \\ w_0 \\ \dot{w}_0 \end{bmatrix} dt + \begin{bmatrix} 0 \\ 1 \\ 0 \\ 0 \end{bmatrix} P(t)dN(t). \quad (37)$$

The state vector defined as $\mathbf{Y}(t) = [\mathbf{q}(t),\ \dot{\mathbf{q}}(t),\ X(t),\ \dot{X},\ w_0(t),\ \dot{w}_0]^T$ is then governed by the following stochastic matrix equation:

$$d\mathbf{Y}(t) = \mathbf{A}\mathbf{Y}(t)dt + \mathbf{b}P(t)dN(t) \quad (38)$$

where $\mathbf{A}$ and $\mathbf{b}$ have the same structure as defined by (26) with the matrices $\mathbf{B}$ and $\mathbf{A}_f$ and vector $\mathbf{b}_f$ defined as

$$\mathbf{B} = \begin{bmatrix} \beta_1^{(3)} & 0 & \gamma_1^{(1)} & \gamma_1^{(2)} \\ \beta_2^{(3)} & 0 & \gamma_2^{(1)} & \gamma_2^{(2)} \\ \dots & \dots & \dots & \dots \\ \beta_N^{(3)} & 0 & \gamma_N^{(1)} & \gamma_N^{(2)} \end{bmatrix} \quad (39)$$

$$\mathbf{A}_f = \begin{bmatrix} 0 & 1 & 0 & 0 \\ -\Omega_f^2 & -2\zeta_f\Omega_f & 0 & 0 \\ 0 & 0 & 0 & 1 \\ 1 & 0 & -\Omega_0^2 & -2\zeta_0\Omega_0 \end{bmatrix}, \quad \mathbf{b}_f = \begin{bmatrix} 0 \\ 1 \\ 0 \\ 0 \end{bmatrix} \quad (40)$$

Using a more simple approach, the motion $w_0(t)$ is assumed to be directly the response of the structure (idealized as a single-degree-of-freedom system) to a Poisson train of impulses, governed by the following equation:

$$\ddot{w}_0(t) + 2\zeta_f\Omega_f\dot{w}_0(t) + \Omega_f^2 w_0(t) = \sum_{i=1}^{N(t)} P_{0i}\delta(t-t_i) \quad (41)$$

Hence, the response $w_0(t)$ is a train of impulse response functions $h_0(t-t_i)$ of the structure given as

$$w_0(t) = \sum_{i=1}^{N(t)} P_{0i} h_0(t-t_i) \tag{42}$$

where impulse response functions $h_0(t-t_i)$ are expressed as

$$h_0(t-t_i) = \frac{1}{\Omega_0\sqrt{1-\zeta_0^2}} \exp\left[-\zeta_0\Omega_0(t-t_i)\right] \sin\left[\Omega_0\sqrt{1-\zeta_0^2}(t-t_i)\right], \quad t > t_i \tag{43}$$

The stochastic counterpart of Eq. (41) is expressed as

$$\begin{aligned} dw_0(t) &= \dot{w}_0(t)dt, \\ d\dot{w}_0(t) &= -2\zeta_0\Omega_0\dot{w}_0(t)dt - \Omega_0^2 w_0(t)dt + P_0(t)dN(t), \end{aligned} \tag{44}$$

where $dN(t) = N(t+dt) - N(t)$ and $P_0(t)$ is the magnitude of the impulse which occurs in the time interval $[t,\ t+dt)$. The matrix form of the stochastic equations of motion (44) is

$$d\begin{bmatrix} w_0 \\ \dot{w}_0 \end{bmatrix} = \begin{bmatrix} 0 & 1 \\ -\Omega_0^2 & -2\zeta_0\Omega_0 \end{bmatrix} \begin{bmatrix} w_0 \\ \dot{w}_0 \end{bmatrix} dt + \begin{bmatrix} 0 \\ 1 \end{bmatrix} P_0(t)dN(t). \tag{45}$$

In that case, the state vector is defined as

$$\mathbf{Y}(t) = \begin{bmatrix} \mathbf{q}(t) & \dot{\mathbf{q}}(t) & w_0(t) & \dot{w}_0(t) \end{bmatrix}^T \tag{46}$$

and is governed by the stochastic Eqs. (38) where

$$\mathbf{A}_f = \begin{bmatrix} 0 & 1 \\ -\Omega_0^2 & -2\zeta_0\Omega_0 \end{bmatrix}, \quad \mathbf{B} = \begin{bmatrix} \gamma_1^{(1)} & \gamma_1^{(2)} \\ \gamma_2^{(1)} & \gamma_2^{(2)} \\ \cdots & \cdots \\ \gamma_N^{(1)} & \gamma_N^{(2)} \end{bmatrix},$$

$$\mathbf{b} = \begin{bmatrix} \mathbf{0} \\ \boldsymbol{\beta}^{(3)} \\ \mathbf{b}_f \end{bmatrix}, \quad \boldsymbol{\beta}^{(3)} = \begin{bmatrix} \beta_1^{(3)} \\ \cdots \\ \beta_N^{(3)} \end{bmatrix}, \quad \mathbf{b}_f = \begin{bmatrix} 0 \\ 1 \end{bmatrix} \tag{47}$$

The equations for the mean values $\mathbf{m}(t) = E[\mathbf{Y}(t)]$ of the response state variables are

$$\frac{d}{dt}\mathbf{m}(t) = \mathbf{A}\mathbf{m}(t) + \nu\mathbf{b}E\left[P_0\right] \tag{48}$$

where $\nu = \text{const}$ is the Poisson process parameter. The equations for second-order joint statistical moments $\mu_{ij}(t) = E[Y_i(t)Y_j(t)]$ of the response variables are formulated with the aid of generalized Itô's differential rule as

$$\dot{\mu}_{ij}(t) = 2\left\{E\left[Y_i(t)a_j(\mathbf{Y}(t))\right]\right\}_s + \nu b_i b_j E[P_0^2], \tag{49}$$

where

$$a_j(\mathbf{Y}(t)) = \sum_k A_{jk}Y_k(t) \tag{50}$$

is the scalar product of the jth row of the matrix $\mathbf{A}$ and $\mathbf{Y}(t)$, and $\{...\}_s$ denotes the Stratonovich symmetrizing operation, e.g.

$$\{Y_i a_j\}_s = \frac{1}{2}(Y_i a_j + Y_j a_i) \tag{51}$$

Eq. (49) can be re-written in the matrix form as

$$\frac{\mathrm{d}}{\mathrm{d}t}\mathbf{R}_{\mathbf{YY}} = \mathbf{A}\mathbf{R}_{\mathbf{YY}} + \mathbf{R}_{\mathbf{YY}}\mathbf{A}^T + \nu\mathbf{b}\mathbf{b}^T E\left[P_0^2\right] \tag{52}$$

where elements of the covariance matrix $\mathbf{R}_{\mathbf{YY}} = E[\mathbf{Y}\mathbf{Y}^T]$ represent the second-order joint statistical moments $\mu_{ij}(t) = E[Y_i(t)Y_j(t)]$.

The model can be simplified further by using a single mode approximation in (6) so that the state vector (46) is expressed in terms of the modal coordinate q_r. In that case the matrix $\mathbf{A}$ and vector $\mathbf{b}$ are defined as

$$\mathbf{A} = \begin{bmatrix} 0 & 1 & 0 & 0 \\ -\omega_r^2 & -2\zeta_r\omega_r & \gamma_r^{(1)} & \gamma_r^{(2)} \\ 0 & 0 & 0 & 1 \\ 0 & 0 & -\Omega_0^2 & -2\zeta_0\Omega_0 \end{bmatrix}; \quad \mathbf{b} = \begin{bmatrix} 0 \\ \beta_r^{(3)} \\ 0 \\ 1 \end{bmatrix} \tag{53}$$

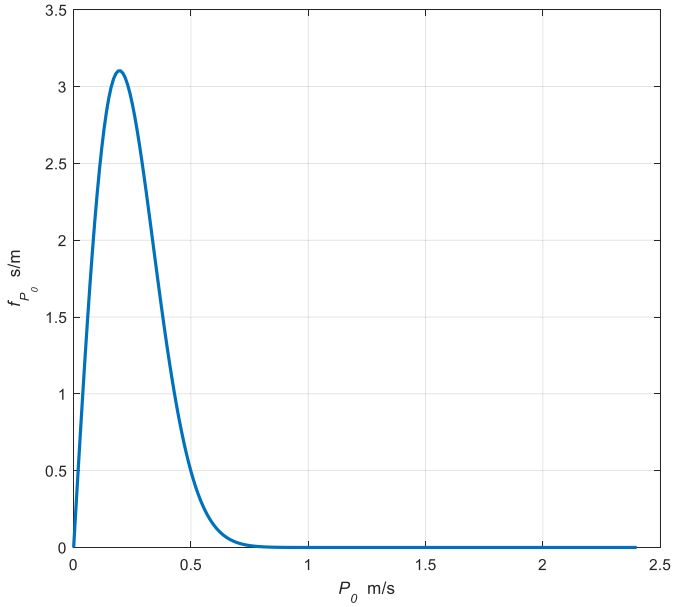

Fig. 3. Rayleigh probability density functions $f_{P_0}(P_0)$ for $\sigma_{P_0} = 0.1954$ m/s.

The equations for second-order joint statistical moments are then expressed as follows:

$$\begin{aligned} \dot{\mu}_{11}(t) &= 2\mu_{12}, \\ \dot{\mu}_{12}(t) &= -\omega_r^2\mu_{11} - 2\zeta_r\omega_r\mu_{12} + \gamma_r^{(1)}\mu_{13} + \gamma_r^{(2)}\mu_{14} + \mu_{22}, \\ \dot{\mu}_{13}(t) &= \mu_{14} + \mu_{23}, \\ \dot{\mu}_{14}(t) &= -\Omega_0^2\mu_{13} - 2\zeta_0\Omega_0\mu_{14} + \mu_{24}, \\ \dot{\mu}_{22}(t) &= -2\omega_r^2\mu_{12} - 4\zeta_r\omega_r\mu_{22} + 2\gamma_r^{(1)}\mu_{23} + 2\gamma_r^{(2)}\mu_{24} + \nu\left(\beta_r^{(3)}\right)^2 E[P_0^2], \\ \dot{\mu}_{23}(t) &= -\omega_r^2\mu_{13} - 2\zeta_r\omega_r\mu_{23} + \gamma_r^{(1)}\mu_{33} + \gamma_r^{(2)}\mu_{34} + \mu_{24}, \\ \dot{\mu}_{24}(t) &= -\omega_r^2\mu_{14} - \Omega_0^2\mu_{23} - 2\left(\zeta_r\omega_r + \zeta_0\Omega_0\right)\mu_{24} + \gamma_r^{(1)}\mu_{34} \\ &\quad + \gamma_r^{(2)}\mu_{44} + \nu\beta_r^{(3)}E[P_0^2], \\ \dot{\mu}_{33}(t) &= 2\mu_{34}, \\ \dot{\mu}_{34}(t) &= -\Omega_0^2\mu_{33} - 2\zeta_0\Omega_0\mu_{34} + \mu_{44}, \\ \dot{\mu}_{44}(t) &= -2\Omega_0^2\mu_{34} - 4\zeta_0\Omega_0\mu_{44} + \nu E[P_0^2]. \end{aligned} \tag{54}$$

In the analysis to follow the impulse magnitudes $P_0(t)$ are assumed to be non-zero mean Rayleigh-distributed random variables [17] with the probability density function given as

$$f_{P_0}(P_0) = \frac{P_0}{\sigma_{P_0}^2} \exp\left(-\frac{P_0}{2\sigma_{P_0}^2}\right) \tag{55}$$

where σ_{P_0} is the Rayleigh distribution parameter. The expected (mean) value is expressed in terms of σ_{P_0} as

$$E\left[P_0\right] = \sigma_{P_0}\sqrt{\frac{\pi}{2}} \tag{56}$$

The corresponding mean square value of P_0 is determined as

$$E\left[P_0^2\right] = 2\sigma_{P_0}^2, \tag{57}$$

Fig. 3 shows the Rayleigh probability density function plot for the Rayleigh distribution parameter $\sigma_{P_0} = 0.1954$m/s. The Rayleigh distribution parameters in Fig. 3 correspond to the mean values $E[P_0] = 0.2449$m/s determined as

$$E\left[P_0\right] = \frac{E\left[A_{\max}\right]}{h_{0\max}}, \tag{57a}$$

where $A_{\max}$ denotes the maximum amplitudes of the host structure sway for a wind with a given statistical Return Period [2]. In the calculations $E[A_{\max}] = A_0 = 0.3$ m and $h_{0\max} = 1.2250$, respectively, are

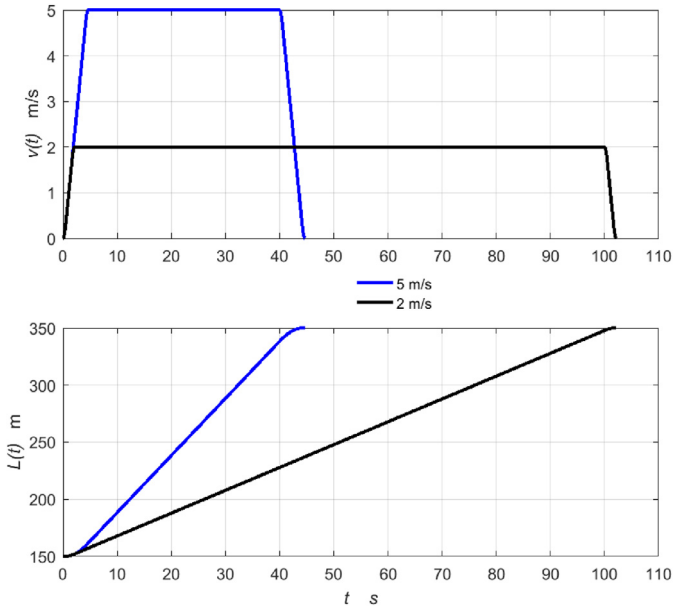

Fig. 4. Speed variation and cable length variation.

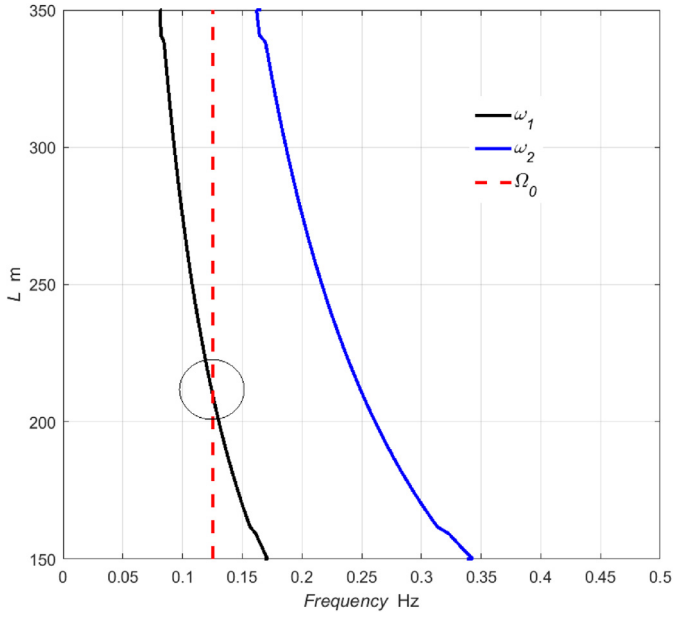

Fig. 5. Variation of the first two natural frequencies of the cable ω_i, $i=1$, 2, for the maximum speed of 5 m/s, together with the frequency of the structure sway $\Omega_0 = 0.125$ Hz (dashed vertical line).

used as determined from Eq. (43) for the time $t_{max} = 1.9688$ s using $\Omega_0 = 0.7854$ rad/s and $\zeta_0 = 0.025$, respectively.

4. Parametric case study: numerical solution and results

The mathematical models developed in this study are formulated in terms of ordinary differential equations with slowly varying coefficients. Due to their nonstationary nature, it is difficult to solve these models by analytical means. However, approximate solutions can be obtained by the application of numerical techniques. In order to assess the usefulness of the models and their ability to predict both the deterministic and stochastic behaviour of the system, a parametric study has been conducted for a cable of mass per unit length $m = 1.3$ kg/m moving at speed upwards and downwards, respectively.

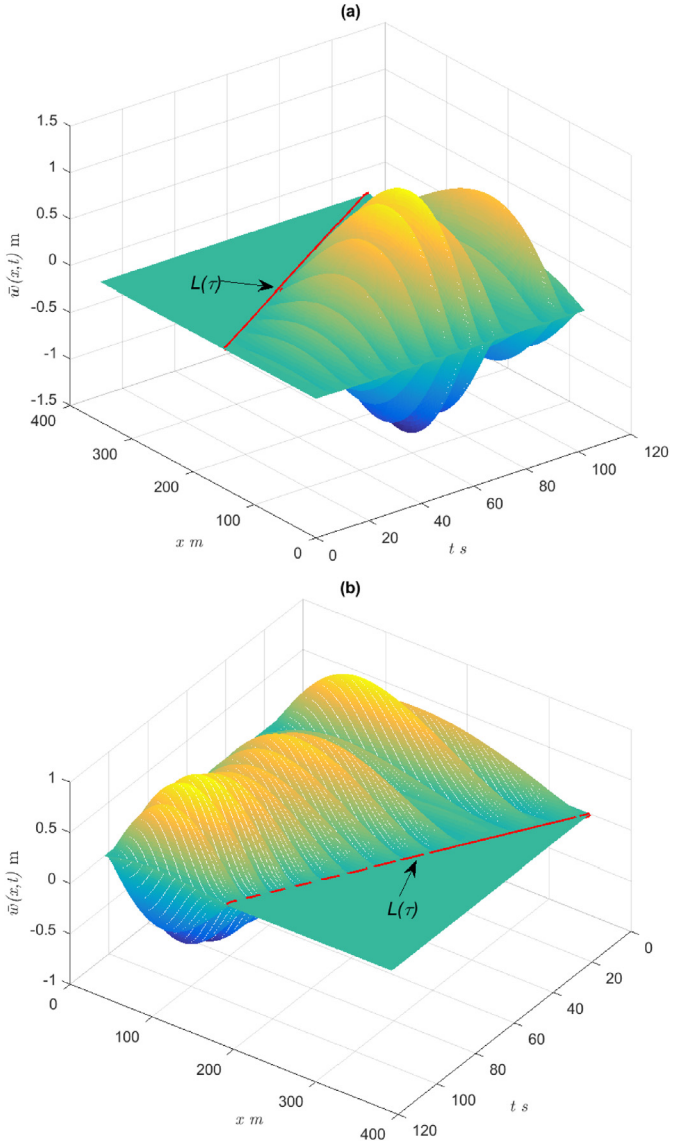

Fig. 6. Deterministic model displacements $\bar{w}(x,t)$ of the cable, $0 \le x \le L(\tau)$, for the frequency of the sway $\Omega_0 = 0.125$ Hz; (a) moving upwards, (b) moving downwards; at the maximum speed of 2 m/s.

The numerical simulation tests have been conducted for various numbers N of terms in the expansion (6). It has been established that to obtain sufficient convergence relatively small numbers of terms are needed and three modes ($N = 3$) have been used in the simulations. In the scenarios considered in this study first the system is ascending from the lower level upwards to the higher level with the travel height of $H = 200$ m. The length of the cable changes from $L(0) = 150$ m to $L_{max} = L(0) + H = 350$ m during the up travel. The upper support B has the maximum speed ranging from 2 m/s to 5 m/s. Fig. 4 shows the variation of velocity $v(t)$ and of the cable length $L(t)$ with time for the maximum speeds of 2 m/s and 5 m/s, respectively. Then, the simulations are carried out for the system descending from the higher level downwards, with the length of the cable changing from $L_{max} = 350$ m to 150 m. The host structure is subjected to the fundamental resonance sway of frequency $\Omega_0 = 0.7854$ rad/s(0.125 Hz) and the amplitude of the sway is $A_0 = 0.75$ m, measured at $z_0 = 402.75$ m above the ground. The cable has a constant mean tension of $T_0 = 2452.5$N and the damping ratios are assumed as $\zeta_r = 3\%$ across all modes.

The natural frequencies of the system are determined by freezing the slowly varying parameters in the matrix of linear coefficients defined

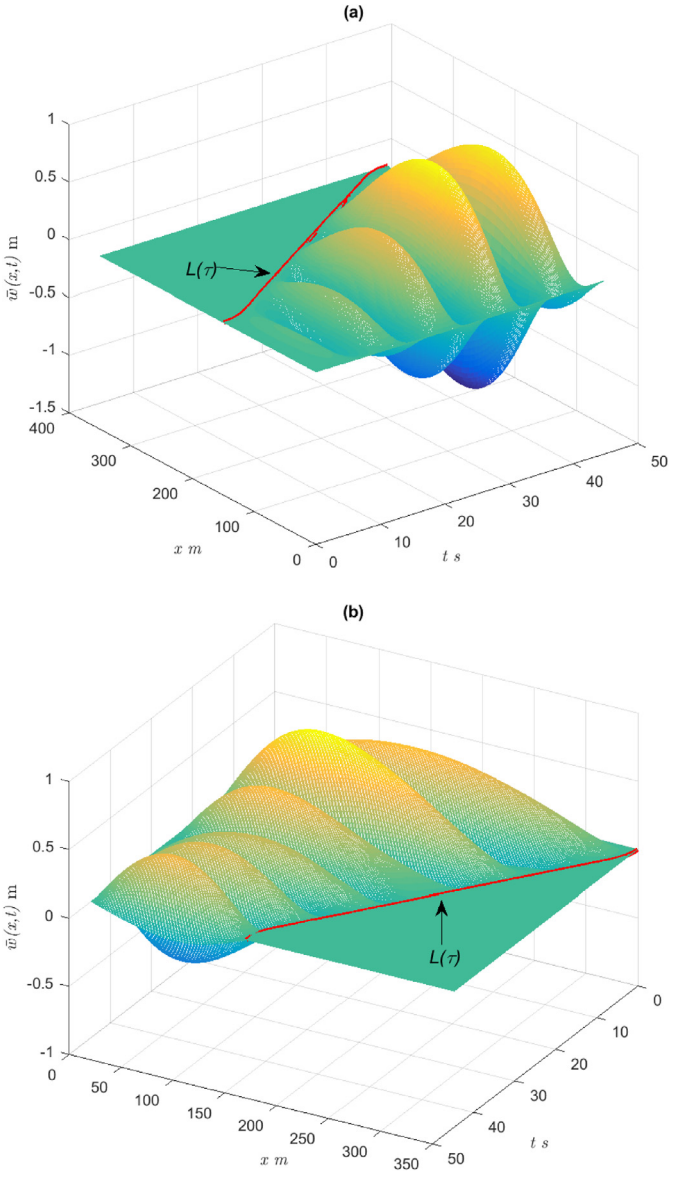

Fig. 7. Deterministic model displacements $\bar{w}(x,t)$ of the cable, $0 \le x \le L(\tau)$, for the frequency of the sway $\Omega_0 = 0.125$ Hz; (a) moving upwards, (b) moving downwards; at the maximum speed of 5 m/s.

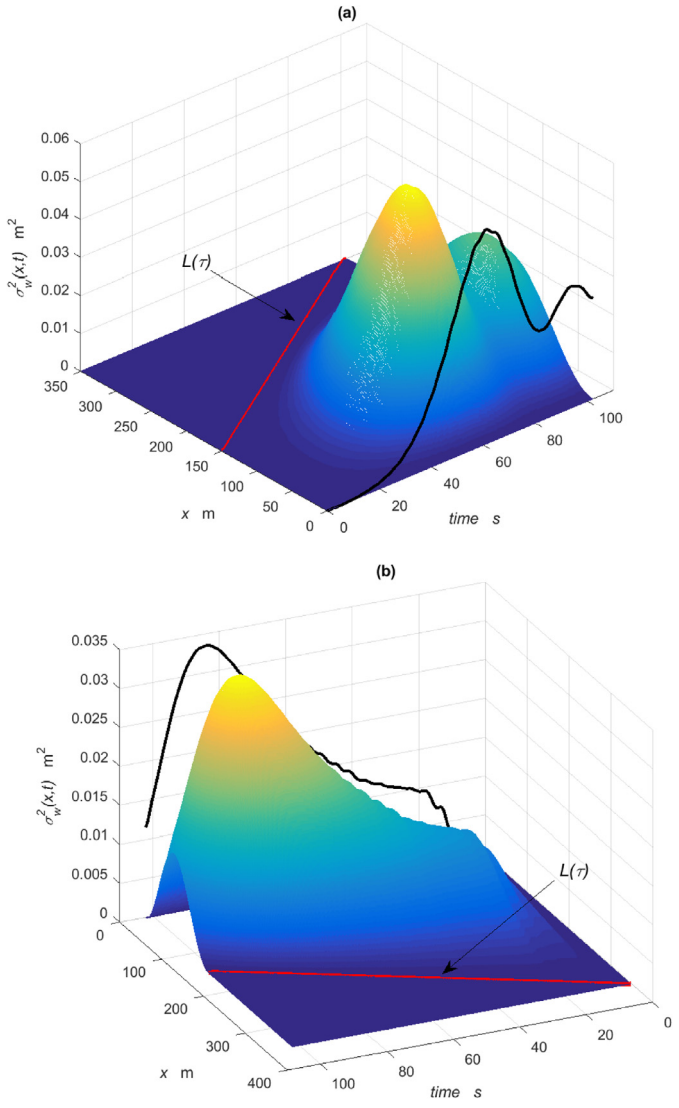

Fig. 8. Gaussian model variance $\sigma_w^2(x,t)$ of the cable response for the maximum speed of 2 m/s, $\Omega_0 = 0.125$ Hz (a) moving upwards; (b) moving downwards; the black curve represents the highest values over time.

by (14) and by solving the eigenvalue problem defined as

$$\mathbf{Az} = \lambda \mathbf{z} \tag{58}$$

where $\mathbf{z} = [\mathbf{q}^T, \dot{\mathbf{q}}^T]^T$ represents the $2N$-dimensional state vector and

$$\mathbf{A} \equiv \mathbf{A}(\tau) = \begin{bmatrix} \mathbf{0} & \mathbf{I} \\ -\mathbf{K}(\tau) & -\mathbf{C}(\tau) \end{bmatrix} \tag{59}$$

where $\mathbf{K}(\tau)$ is a symmetric matrix of coefficients $K_{rn}(\tau)$ and $\mathbf{C}(\tau)$ is a skew-symmetric matrix of coefficients $C_{rn}(\tau)$ defined in (14), respectively. The natural frequencies of the system $\omega_r(\tau)$,$r = 1, 2, \ldots, N$, are then given by imaginary parts of the complex eigenvalues $\lambda_r(\tau)$.

The plot presented in Fig. 5 shows the variation of the first two natural frequencies vs. length of the cable in the scenario when the upper support moves upwards with the velocity profile corresponding to the maximum speed of 5 m/s. The frequency of the structure is represented in this plot by the vertical dashed line. The plots demonstrate that the frequency of the structure ($\Omega_0 = 0.125$ Hz) matches the fundamental frequency of the cable when its length is about 210.3 m, and a passage through the fundamental resonance takes place in this region (the encircled area).

4.1. Deterministic model simulation results

The deterministic dynamic behaviour of the system is described by the discretized equations of motion Eq. (13). In order to determine the response of the cable to the excitation due to the structure sway during the downwards and upwards travel equations (13) are solved numerically by the application of an explicit Runge–Kutta (4,5) formula.

The corresponding dynamic responses of the cable are then calculated from Eq. (6) and are illustrated in Figs. 6 and 7 for the speeds of 2 m/s and 5 m/s, respectively. The dynamic displacements $\bar{w}(x,t)$ are illustrated in subplots (a) and (b) in the space–time domain, for the up/down travel, respectively.

It is evident that when the cable is travelling upwards, with its length increasing (and with the natural frequencies getting decreased), the displacements increase when the resonance region is being approached and after the maximum level is attained they decrease slowly.

In the scenario when the direction of travel is down, the length decreases. After the initial large transient displacements, the response

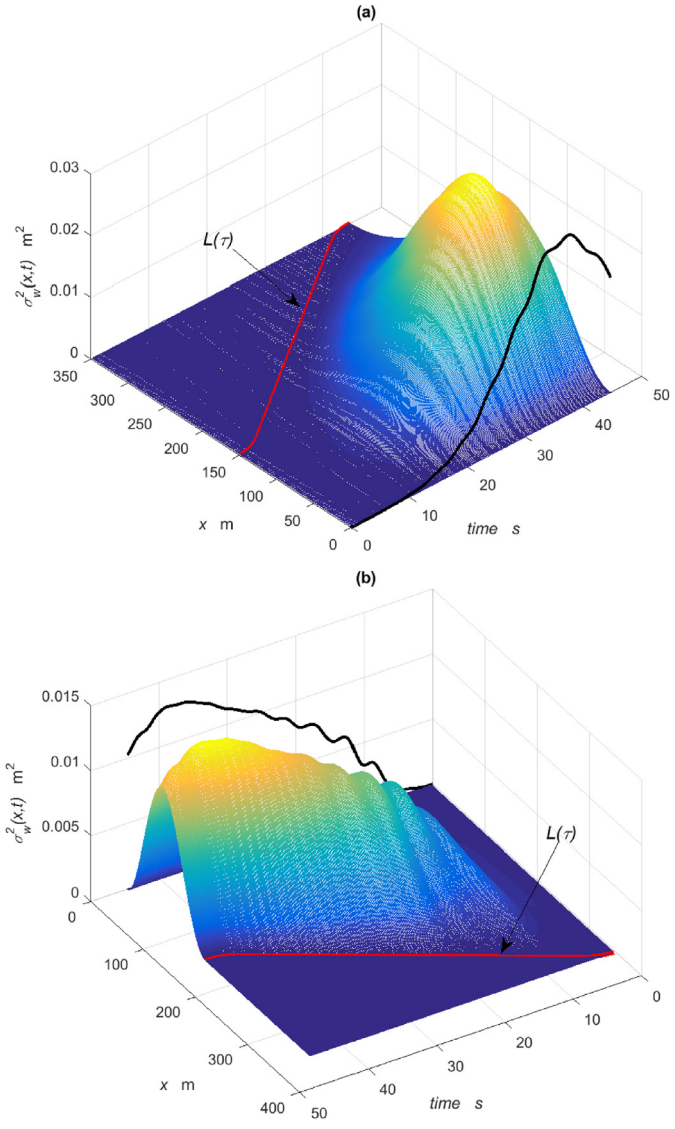

Fig. 9. Gaussian model variance $\sigma_w^2(x,t)$ of the cable response for the maximum speed of 5 m/s, $\Omega_0 = 0.125$ Hz: (a) moving upwards; (b) moving downwards.

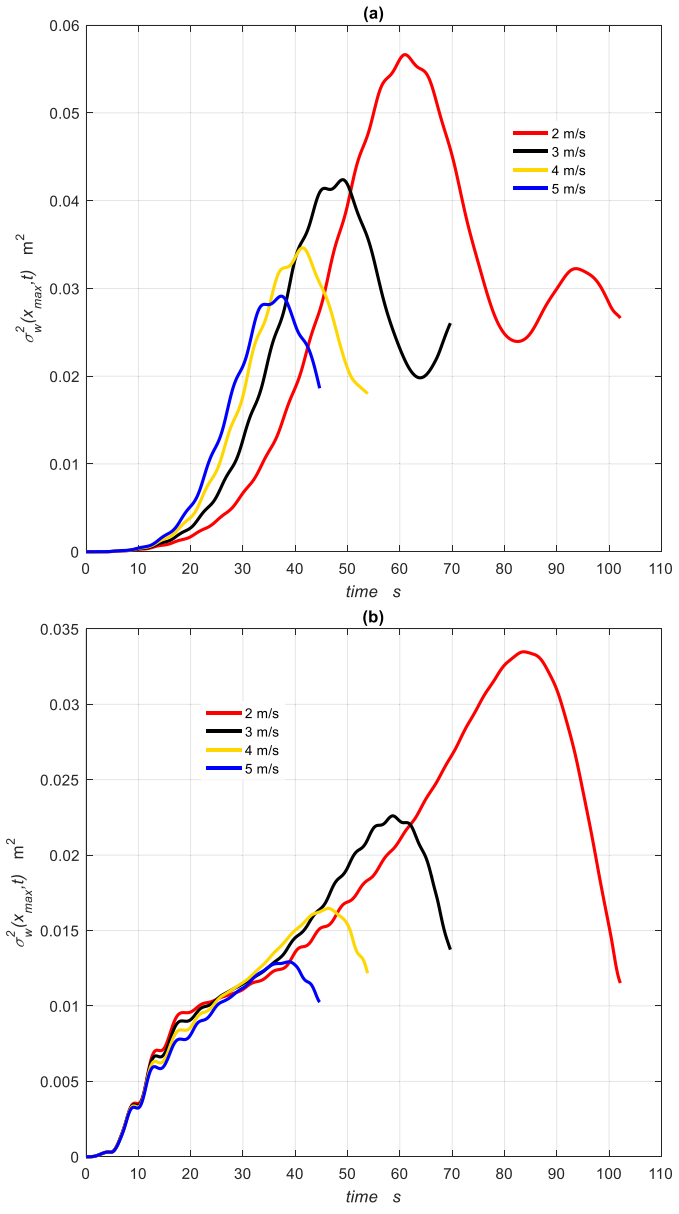

Fig. 10. Gaussian model maximum values of variance $\sigma_w^2(x,t)$ of the cable response vs. time, $0 \le x \le L(\tau)$ for the frequency of the sway $\Omega_0 = 0.125$ Hz (a) moving upwards (b) moving downwards, at the maximum speeds of 2 m/s, 3 m/s, 4 m/s and 5 m/s.

during the passage through resonance demonstrates similar characteristics during the passage through resonance region but the amplitudes are smaller.

It is interesting to observe that the displacement amplitude maxima are delayed and occur later, when the natural frequencies are lower or higher, during travel upwards or downwards, respectively. Similar effects are evident in the results obtained from the stochastic models as discussed in what follows.

4.2. Narrow-band Gaussian stochastic model simulation results

In order to investigate the behaviour of the system acted on by base excitation represented by the narrow-band Gaussian stochastic model the explicit Runge–Kutta (4,5) formula is used to integrate the differential Eq. (29). The filter variable α is determined by Eq. (18) where the constant level of the power spectrum of white noise is assumed as $S_0 = 1$W/Hz. The damping ratio of the second order auxiliary filter is taken as $\zeta_f = 0.025$ in the numerical simulations. In this formulation the second order filter equation in (15) represents the structure subjected to the excitation process *X(t)* (a so called Ornstein–Uhlenbeck process [9]).

Figs. 8 and 9 show the variance functions $\sigma_w^2(x,t)$ determined from Eq. (30) representing the measure of the statistical scatter of the lateral displacements $\bar{w}(x,t)$ for velocity profiles of the maximum speeds of 2 m/s and 5 m/s, respectively. The subplots (a) illustrate the variance for the upwards motion and the subplots (a) show the variance for the downwards motion, respectively. The variance of response changes with time along the cable span when its length is varying Thus, the spatial coordinate x is defined in a slowly time-variant domain $0 < x < L(\tau)$ with the red lines representing the slowly varying length $L(\tau)$. The curves in black line show how the highest values of variance change with time.

It is evident that the variance depends on the direction of travel and the maximum values are higher during the up travel. This is more evident from Fig. 10 where the maximum values are plotted against time for the maximum speeds of 2 m/s, 3 m/s, 4 m/s and 5 m/s, for the up travel in subplot (a) and for the down travel in subplot (b), respectively. It is interesting to note that during the travel, the maximum variance curves rise first reaching their peak values and then the curves fall until the end time.

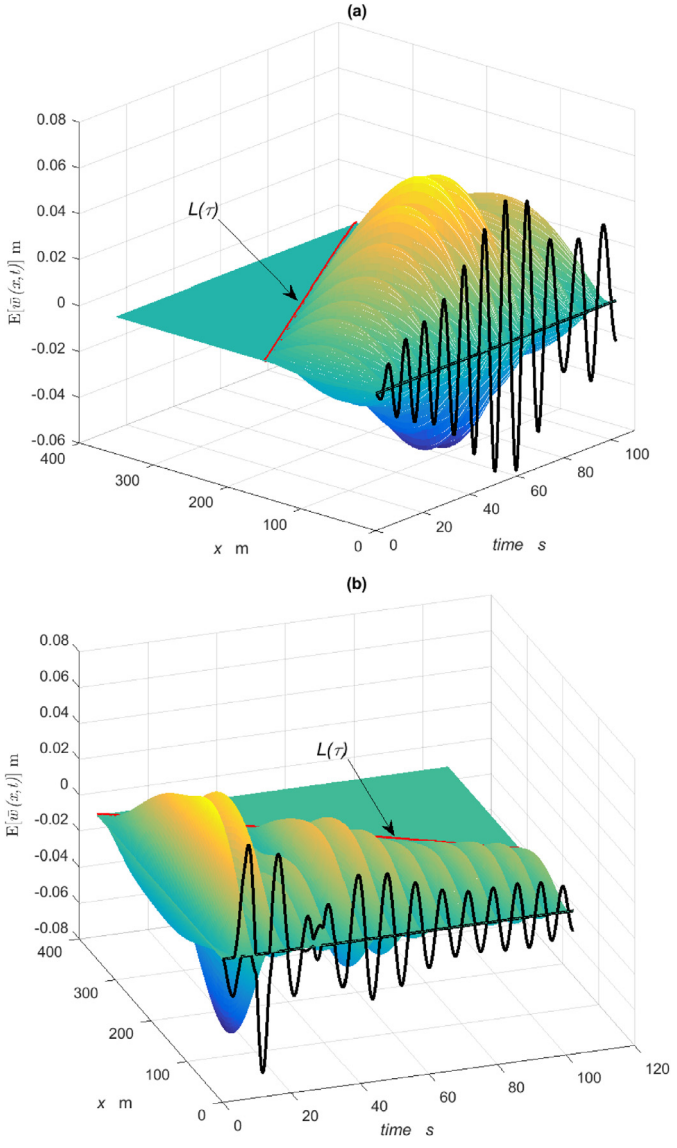

Fig. 11. Non-Gaussian model mean value displacements $E[\bar{w}(x,t)]$ of the cable, $0 \le x \le L(\tau)$, for the frequency of the sway $\Omega_0 = 0.125$ Hz (a) moving upwards (b) moving downwards, at the maximum speed of 2 m/s (the black line shows the peak values).

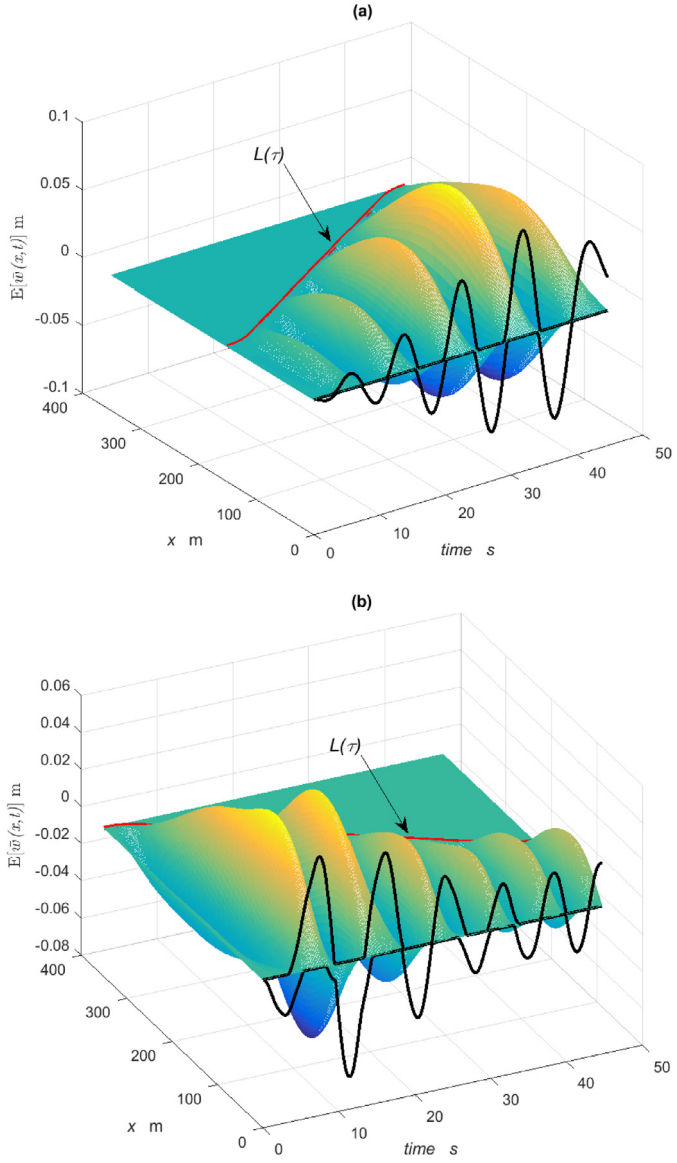

Fig. 12. Non-Gaussian model mean value displacements $E[\bar{w}(x,t)]$ of the cable, $0 \le x \le L(\tau)$, for the frequency of the sway $\Omega_0 = 0.125$ Hz; (a) moving upwards (b) moving downwards, at the maximum speed of 5 m/s.

There is analogy with the deterministic results. The variance maxima occur during the passage through resonance, when the frequency of the structure is near the fundamental frequency of the cable. The effects are however delayed and occur when the natural frequencies are lower or higher, during travel upwards or downwards, respectively.

It is evident that for both directions the higher the speed the lower the scatter levels of the response. This behaviour pattern is consistent with the fact that the faster the passage through the resonance region where the central frequency Ω_0 coincides with the fundamental natural frequency of the cable, the lower the resonance responses.

4.3. Non-Gaussian random pulse train stochastic model simulation results

The mean values $E[\bar{w}(x,t)]$ and the variance $\sigma^2_{\bar{w}}(x,t)$ of the cable displacements $\bar{w}(x,t)$ corresponding to the non-Gaussian model, when the structure motion is treated as a random train of pulses, are shown in Figs. 11–15. Those results are obtained by the numerical integration of Eqs. (48) and (52), with the variance functions determined then from Eq. (30), respectively. The damping ratio of the structure is assumed as $\zeta_f = 0.025$ and $\sigma_{P_0} = 0.1954$m/s is used in the numerical simulation tests. Eq. (54) where the single mode approximation of the cable dynamics is used can be applied for a more rapid estimation of the response variance.

Figs. 11 and 12 demonstrate the mean values in the space–time domain, where the space variable is within the slowly varying domain $0 \le x \le L(\tau)$, for the maximum speeds of 2 m/s and 5 m/s, up travel and down travel, respectively. The plots in Figs. 11 and 12 show also the envelopes of maximum mean values and it is evident that the maximum values depend on the direction of travel and speed. During the travel upwards the mean response initially increase and then it is getting decreased with time. At the higher speed the mean response tends to reach higher values. During downwards travel, when the length of the cable decreases slowly, the mean response values are getting smaller with time.

Figs. 13 and 14 show the variance functions for velocity profiles of the maximum speeds of 2 m/s and 5 m/s, respectively. The subplots (a) illustrate the variance for the upwards motion and the subplots (a) show the variance for the downwards motion, respectively. The curves in black line show how the highest values of variance change with time. There are some strong similarities to the behaviour observed for the

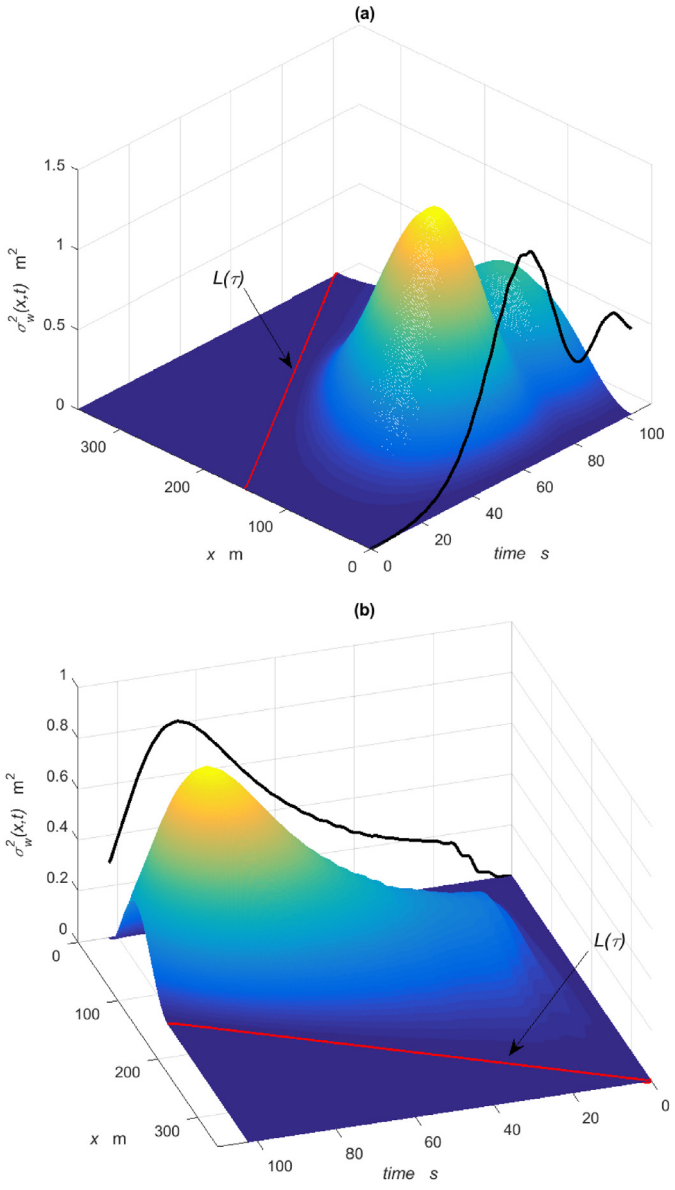

Fig. 13. Non-Gaussian model variance $\sigma_w^2(x,t)$ of the cable response for the maximum speed of 2 m/s, $\Omega_0 = 0.125$ Hz: (a) moving upwards; (b) moving downwards.

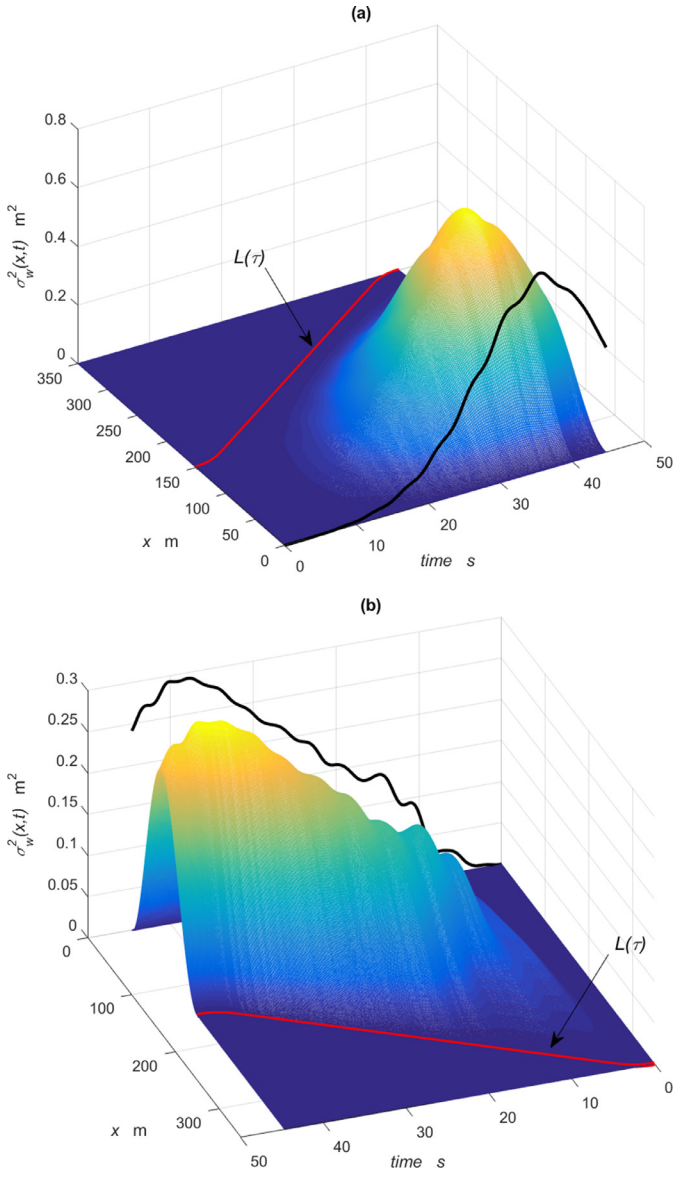

Fig. 14. Non-Gaussian model variance $\sigma_w^2(x,t)$ of the cable response for the maximum speed of 5 m/s, $\Omega_0 = 0.125$ Hz: (a) moving upwards; (b) moving downwards.

Gaussian model as illustrated in Figs. 8 and 9. It is evident that the variance depends on the direction of travel and the maximum values are higher during the up travel. This is more evident from what is shown in Fig. 15 where the maximum values are plotted against time for the maximum speeds of 2 m/s, 3 m/s, 4 m/s and 5 m/s, for the up travel in subplot (a) and for the down travel in subplot (b), respectively. As in the case of Gaussian model it is evident that in both cases the higher the speed the lower the scatter levels of the response. During the travel, the maximum variance curves rise first reaching their peak values and then the curves fall until the end time.

As in the case of the Gaussian model the maxima occur during the passage through resonance, with the effects being delayed during the passage. It is evident that the non-Gaussian model predicts higher values of variance of the response of the cable.

5. Conclusions

Two stochastic models of motion of the structure have been considered. In the first model, the excitation mechanism is represented as a narrow-band process mean-square equivalent to the harmonic process. Due to the demand that the function defining motion of the structure must be continuous its stochastic variation is modeled by filtering of Gaussian white noise through a first order filter followed by a filtration through a second order filter.

In the second model, the random train of pulses representing the excitation due the structure motion is idealized as non-Gaussian process in form of a train of randomly occurring pulses. Then, the equations governing the second-order joint statistical moments of the response are derived.

The models have been used to predict the probabilistic characteristics of the lateral dynamic motions of a long cable moving at speed within a tall host structure. The resulting systems of linear ordinary equations are nonstationary and can be solved by numerical integration. This leads to the determination of covariance matrix with its elements showing the statistical scatter of the response of the system.

The solution procedure is demonstrated through a parametric case study involving the cable moving at speed upwards and downwards within the tall structure. It is shown that the models can be used to investigate the influence of speed on the stochastic response characteristics

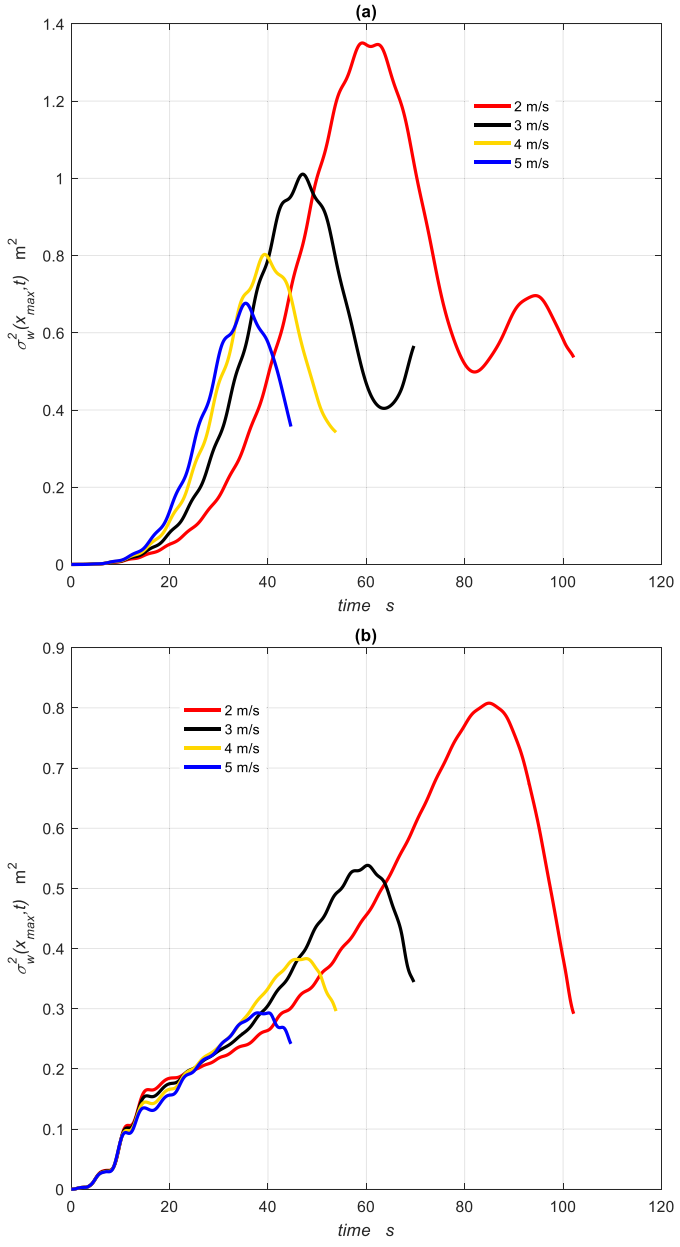

Fig. 15. Non-Gaussian model maximum values of variance $\sigma_w^2(x,t)$ of the cable response vs. time, $0 \le x \le L(\tau)$ for the frequency of the sway $\Omega_0 = 0.125$ Hz (a) moving upwards (b) moving downwards, at the maximum speeds of 2 m/s, 3 m/s, 4 m/s and 5 m/s.

of the system. The numerical results for both models show similarities and demonstrate that the higher the speed the lower the variance of the cable response. However, the non-Gaussian model predictions show higher values of the cable response variance.

Moving slender continua such as suspension ropes and compensating cables are pivotal components of high-rise high-speed modular systems, such as elevators, deployed in tall building structures. The phenomena predicted by the application of the models and the results presented in this paper are consistent with the behaviour of cables observed in practical installations [3]. The proposed methodology and models allow the designer to determine the variance of lateral displacements of these continua in order to establish bounds for their dynamic responses.

References

[1] Cook NJ. The designer's guide to wind loading of building structures part 1. London: Butterworths; 1985.
[2] Kijewski-Correa T, Pirinia D. Dynamic behavior of tall buildings under wind: insights from full-scale monitoring. Struct Des Tall Spec Build 2007;16:471–86.
[3] Strakosch GR. The vertical transportation handbook. New York: John Wiley; 1998.
[4] Terumichi Y, Ohtsuka M, Yoshizawa M, Fukawa Y, Tsujioka Y. Nonstationary vibrations of a string with time-varying length and a mass–spring system attached at the lower end. Nonlin Dyn 1997;12:39–55.
[5] Salamaliki-Simpson R, Kaczmarczyk S, Picton P, Turner S. Non-linear modal interactions in a suspension rope system with time-varying length. Appl Mech Mater 2006;5–6:217–24.
[6] Kaczmarczyk S, Picton PD. The prediction of nonlinear responses and active stiffness control of moving slender continua subjected to dynamic loadings in vertical host structures. Int J Acoust Vib 2013;18:39–44.
[7] Sandilo SH, van Horssen WT. On a cascade of autoresonances in an elevator cable system. Nonlin Dyn 2015;80:1613–30.
[8] Gaiko NV, van Horssen WT. On transversal oscillations of a vertically translating string with small time-harmonic length variations. J Sound Vib 2016;383:339–48.
[9] Larsen JW, Iwankiewicz R, Nielsen SRK. Probabilistic stochastic stability analysis of wind turbine wings by Monte Carlo simulations. Probab Eng Mech 2007;22:181–93.
[10] Lin-lin Z, Jie L, Yongbo P. Dynamic response and reliability analysis of tall buildings subject to wind loading. J Wind Eng Ind Aerodyn 2008;96:25–40.
[11] Kaczmarczyk S, Iwankiewicz R, Terumichi Y. The dynamic behaviour of a non-stationary elevator compensating rope system under harmonic and stochastic excitations. J Phys Conf Ser 2009;181:012047.
[12] Cornell CA. Stochastic process models in structural engineering. Technical Report 34. Stanford CA: Department of Civil Engineering, Stanford University; 1964.
[13] Merchant DH. Stochastic model of wind gusts. Technical Report 48. Stanford CA: Department of Civil Engineering, Stanford University; 1964.
[14] Racicot R, Moses F. Filtered Poisson process for random vibration problems. J Eng Mech Div ASCE 1972;98:159–76.
[15] Kaczmarczyk S. The passage through resonance in a catenary-vertical cable hoisting system with slowly varying length. J Sound Vib 1997;208:243–69.
[16] Iwankiewicz R, Nielsen SRK. Advanced methods in stochastic dynamics of non-linear systems. Aalborg: University Press; 1999.
[17] Iwankiewicz R. Dynamical mechanical systems under random impulses. World Scientific; 1995.